Effect of non-magnetic and magnetic trivalent ion substitutions on BaM-ferrite properties synthesized by hydrothermal method

Tayssir Ben Ghzaiel, Wadia Dhaoui, Alexandre Pasko, Frédéric Mazaleyrat

Effect of Non-Magnetic and Magnetic Trivalent Ion Substitutions on BaM-Ferrite Properties Synthesized by Hydrothermal Method

Tayssir BEN GHZAIEL[a,b,*], Wadia DHAOUI[a] , Alexandre PASKO[b], Frédéric MAZALEYRAT[b]

[a] Université de Tunis El Manar Faculté des Sciences de Tunis, UR11ES18 Unité de Recherche de Chimie Minérale Appliquée, 2092, Tunis, Tunisie

[b] SATIE, ENS Cachan, CNRS, Université Paris-Saclay, 61 av du Président Wilson, F-94230 Cachan, France

*Corresponding author. Tel. +33 7 54 04 91 18

E-mail address: tayssir.ben-ghzaiel@satie.ens-cachan.fr

GRAPHICAL ABSTRACT

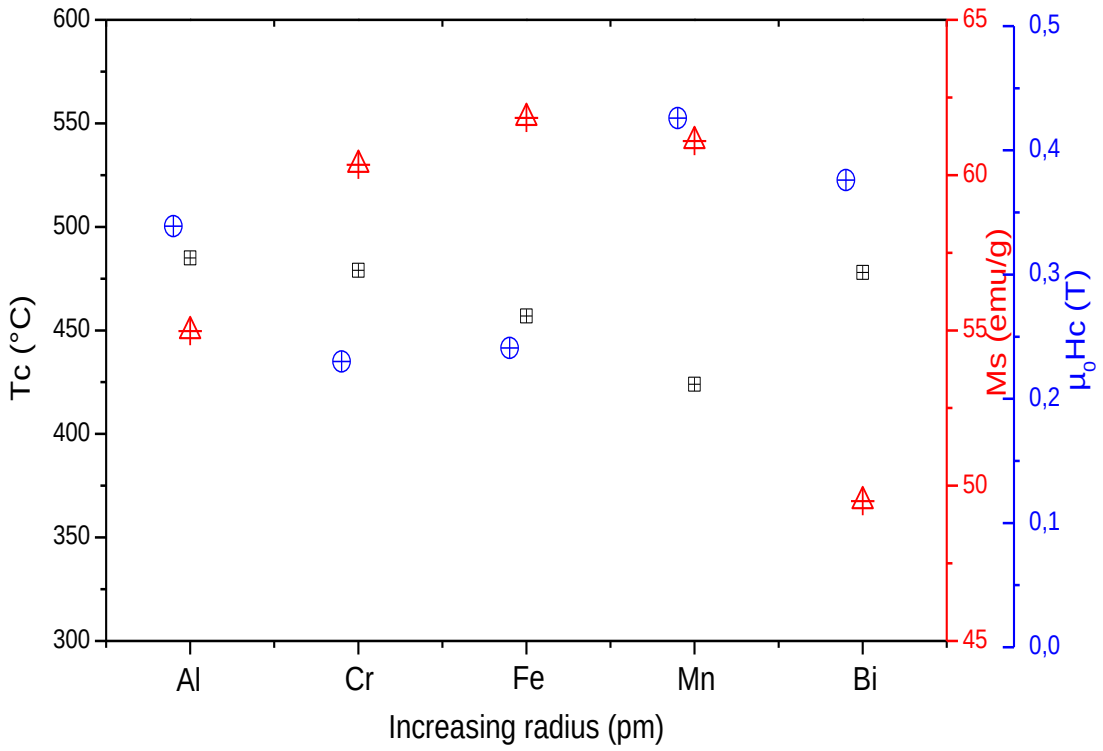

Abstract

Two spices trivalent transition metal ions, nonmagnetic Al^{3+}, Bi^{3+} and magnetic Cr^{3+}, Mn^{3+} substituted barium hexaferrite powders are synthesised via dynamic hydrothermal method then calcinated at different temperatures. Powder XRD patterns analysis and Rietveld refinement indicate magnetoplumbite-type crystalline phase. The crystallite size calculated using Scherer's formula varies from 153 to 248 nm as it is affected by the ionic radius of trivalent metal ions and calcination temperatures. The morphological features show agglomerations of spherical-shaped particles with an average size of 400 ± 50 nm for $BaBiFe_{11}O_{19}$ and hexagonal-shaped particles 1-2µm for the other substitutions. Magnetic studies show a ferromagnetic behaviour for all samples. The nonmagnetic Al^{3+}, Bi^{3+} substituted materials have lower saturation magnetization Ms and remanence Mr than the magnetic substitutions Cr^{3+}, Mn^{3+}. These results reveal that Ms and Mr are related to the magnetic moment of each metallic ion and its distribution in the lattice. For magnetic substitution, Ms of manganese substitution (61.10 emu/g) is found higher than that of chromium (60.33 emu/g) since Mn^{3+} has a magnetic moment of $5\mu_B$ greater than Cr^{3+} with $3\mu_B$. Coercivity Hc and maximum energy product $(BH)_{max}$ determined from M-H loops exhibit an increasing trend with calcination temperature as they are related to the crystallite size. Hc and $(BH)_{max}$ of $BaMnFe_{11}O_{19}$ are found maximum 0.426 T and 7.47 $kJ.m^{-3}$, respectively.

Keywords: Magnetically ordered materials; Crystal structure; Magnetisation; Magnetic measurement; Scanning electron microscopy, SEM; X-ray diffraction.

1. Introduction

Ferrimagnetic oxides have received considerable attention in the few last decades owing to their remarkable magnetic characteristics such as high Curie temperature, large permeability, high saturation magnetization and magnetocristalline anisotropy [1]. The diverse magneto-electric properties displayed by these materials have given rise to a great variety of compounds for technological and industrial applications [2].

Ferrites are ferrimagnetic oxides divided into three families: spinel, garnet and hexagonal. Among the family of hexagonal ferrite, barium hexaferrite $BaFe_{12}O_{19}$ (BaM) with magnetoplumbite structure (P63/mmc) is well known as hard magnetic material with strong magnetocristalline anisotropy along c-axis, high Curie temperature (Tc= 472 °C), relatively high magnetization saturation, high electrical resistivity, chemical stability and resistance to corrosion [3]. These properties arise from exchanges between the oxygen and metallic ions occupying particular positions in its hexagonal crystalline structure.

Several investigations on the substituted barium ferrite have been carried out to further improve its magnetic and electrical properties. A proper cation substitution on iron ions, in tetrahedral and octahedral site of BaM unit cell, by trivalent magnetic or nonmagnetic metal ions or with appropriate arrangement of bivalent and tetravalent cations is an effective way to change these properties [4-9]. When metal ions are incorporated in BaM compound, its saturation magnetization, coercivity and anisotropy field depend on the nature, combination and distribution of this substitution in Fe sublattices.

The aim of the present work is to study the chemical changes that can be induced by the nature and distribution of the trivalent ion in barium hexaferrite and the resulting

magnetic properties. Two species of trivalent ions are selected, nonmagnetic ions Al^{3+}, Bi^{3+} and magnetic ions Cr^{3+}, Mn^{3+} ions for Fe^{3+} substitution within $BaFe_{12}O_{19}$ compound. To examine the influence of the incorporation of each substitution on BaM ferrite and find out the chemical structure modifications, X-ray diffraction, FTIR spectroscopy, SEM and EDX analysis are used. The effects of the trivalent ions substitution and its correlation with magnetic behaviour of these hexaferrites are then investigated.

2. Experimental

2.1. Chemicals

Starting materials $Fe(NO_3)_3.9H_2O$, $Ba(NO_3)_2$, $Al(NO_3)_3.9H_2O$, $Bi(NO_3)_3.5H_2O$, $Cr(NO_3)_3.9H_2O$, $Mn(NO_3)_2.4H_2O$ and NaOH used as such without any further treatment, for the synthesis of different samples, are purchased from Sigma-Aldrich.

2.2. Material preparation

Samples of Ba*Me*$Fe_{11}O_{19}$ (*Me* =Al, Bi, Cr and Mn) hexaferrites are prepared by dynamic hydrothermal method. Appropriate amount of $Fe(NO_3)_3.9H_2O$, $Ba(NO_3)_2$, $Al(NO_3)_3.9H_2O$ or $Bi(NO_3)_3.5H_2O$ or $Cr(NO_3)_3.9H_2O$ or $Mn(NO_3)_2.4H_2O$ are mixed with 2.5 $mol.L^{-1}$ NaOH solution according to desired stoichiometries, at room temperature and under magnetic stirring. The resulting solution is poured into teflon-lined stainless steel autoclave which is sealed, then placed in a shaked furnace. The autoclave is maintained at 220 °C for 8 h, then cooled down to room temperature. The obtained products are filtered, washed several times with distilled water and finally dried in an oven at 80 °C.

The processed powders are calcined in air in the temperature range from 900 °C to 1000 °C for 2 h with heating rate of 10 °C.min^{-1}. The details of different samples are summarized in Table 1.

2.3. Characterization

The phase composition and structure of the synthesized samples are examined using PANalytical X'Pert Pro diffractometer with Cobalt Kα radiation (λ = 1.79 Å) in the range of 10° ≤ 2θ ≤ 80° with 0.02° step size. Crystal structure and microstructure are refined applying Rietveld method using MAUD software [10]. Structural parameters such as lattice constants (*a* and *c*) and crystallite size *D* are obtained from Rietveld analysis. The unit volume cell *V* and X-ray density ρ_{XRD} of the prepared samples are calculated by the following equations

$$\boldsymbol{V = \frac{\sqrt{3}}{2}\, a^2\, c} \quad (1)$$

$$\boldsymbol{\rho_{XRD} = \frac{Z\, M}{N_A\, V}} \quad (2)$$

where *d* is the distance between lattice planes and (*h*, *k*, *l*) Miller indices, *Z* the number of formula units in a cell, M the molar mass of the sample and N_A Avogadro number.

Infrared spectra of different samples are obtained on a Thermo Electron Corporation Nicolet Nexus 670 FTIR Spectrometer, collecting 64 scan in the range of 4000 - 400 cm^{-1}, with 4 cm^{-1} resolution at room temperature. The surface morphology and EDX analysis are studied using scanning electron microscope (SEM) Hitachi S-3400N model equipped with TEAM™ EDX system for elemental microanalysis. The spectra of the samples are collected by smart phase mapping to provide high level of elemental analysis. Magnetic measurements, such as saturation magnetization Ms,

remanent magnetization Mr, coercivity Hc and Curie temperature Tc are made on Lake Shore 7400 vibrating sample magnetometer (VSM).

3. Results and discussion

3.1. X-ray structure analysis

The powder X-ray diffraction patterns of Ba*Me*$Fe_{11}O_{19}$ samples with *Me* = Al, Bi, Cr and Mn annealed at 900, 950, 1000 °C are presented in Fig. 1. All the sharp reflection peaks are indexed corresponding to the standard data obtained from M-type barium hexaferrite ICDD pattern No. 74-1121 within space group P63/mmc. For different samples, $BaFe_{12}O_{19}$ phase is formed at 900 °C together with other secondary phases. The amount of the main phase increases with increasing temperature, while other phases decease or disappear.

Lattice parameters (*a* and *c*), crystallite size (*D*) and the X-ray density (ρ_{XRD}) of the substituted hexaferrites are calculated and their values are listed in Table 2. It can be seen that with increasing calcination temperature from 900 to 1000 °C, an increase of crystallite size is induced. The X-ray density decreased for $BaAlFe_{11}O_{19}$, $BaCrFe_{11}O_{19}$ and $BaMnFe_{11}O_{19}$, whereas, it increased for $BaBiFe_{11}O_{19}$ since it is related to the molecular weight.

As shown in Table 2, lattice constants of the hexaferrite samples are affected by radius of the substitution ion. In fact, for $BaAlFe_{11}O_{19}$, $BaCrFe_{11}O_{19}$ and $BaMnFe_{11}O_{19}$ ferrite, *a* and *c* are similar to those of $BaFe_{12}O_{19}$ as the ionic radius values of Al^{3+}, Cr^{3+} and Mn^{3+} are close to that of Fe^{3+} (see Table 3, [11, 12]), so, it is easier to substitute in the lattice of barium ferrite [13-16]. However, they did not change with bismuth substitution as it is thought. Actually, it is supposed that Bi^{3+} (radius = 96 pm) could be

oxidized to Bi^{5+} (radius = 74 pm), to substitute the Fe^{3+} ions (radius = 67 pm) in hexagonal phase. As Bi^{3+} cation is unstable in Fe^{3+} sites, the following chemical reaction may result:

$$Bi^{3+} + 2\ Fe^{3+} \longrightarrow Bi^{5+} + 2\ Fe^{2+}$$

So, for each Bi^{5+} entering the lattice two Fe^{2+} are formed [17].

3.2. Infrared analysis

The formation of the hexagonal structure of substituted barium ferrite is also investigated by infrared analysis. Typical FTIR spectra of $BaFe_{12}O_{19}$, Al1000, Bi1000, Cr1000 and Mn1000 are shown in Fig. 2. For all samples, the spectra indicate the presence of absorption bands in the range of 400 to 800 cm^{-1} which are a common feature of the hexaferrites [18]. The lower frequency absorption band ν_1 between 400 and 490 cm^{-1} is assigned to Fe-O bending vibration of octahedral site and the higher frequency absorption band ν_2 lying in the range of 500 to 600 cm^{-1} is related to Fe-O stretching vibration in the tetrahedral site [19]. The ν_1 and ν_2 bands continuously increase with annealing temperature from 900 °C to 1000 °C which reflect the presence of high degree of crystallinity. No other band is observed, suggesting that single $BaFe_{12}O_{19}$ phase is obtained which is in agreement with XRD characterization. For pure hexaferrite, the remarkable absorption peak at 545 cm^{-1} is associated to Ba-O stretching vibration band [20]. This peak is less observed in the substituted ferrites, since it is overlapped with the characteristic bands (ν_1 and ν_2) of hexaferrite [21]. The bands in the range of 1000 - 1700 cm^{-1} are associated to Metal-Oxygen-Metal bands [22], whereas, the broad band around 3400 cm^{-1} is due to the adsorbed water molecules. For pure $BaFe_{12}O_{19}$, it can be observed that there is an even distribution of iron ions in the two

sites since the absorbance of ν_1 and ν_2 bands are alike. This tendency changes with substituted hexaferrites. For aluminium, chromium and manganese substitution, absorbance of stretching vibration in the tetrahedral site ν_2 becomes greater than that of bending vibration of octahedral site ν_1, however, the absorbance of ν_2 is lower than that of ν_1 for $BaBiFe_{11}O_{19}$, independently of the calcination temperature. This phenomenon can be related to the mass of the atoms since heavier atoms vibrate slower than lighter ones, so Me-O band will vibrate at a lower frequency therefore the stretching absorption will be decreased for bismuth compared to other hexaferrites. Other reason may be related to the radius of trivalent ion. In fact, Al^{3+}, Cr^{3+} and Mn^{3+} have ionic radius close to that Fe^{3+}, so a tendency to replace the tetrahedral sites except for manganese which can be in all sites. But by examining its IR spectrum, it occupies preferentially the tetrahedral site. Bi^{3+} with its large radius trends to occupy the octahedral site, as seen from lattice parameters determined from XRD study. So, increasing bending vibration of this site by bismuth increased its dimension, so its absorbance [23].

3.3. Morphological analysis

The surface morphology and microstructure of Al1000, Bi1000, Cr1000 and Mn1000 are observed by scanning electron microscopy (SEM) as depicted in Fig. 3. Agglomerated hexagonal shaped particles can be observed in all four samples. Bi1000 reveals small spherical shaped-particles with a size about 400 ± 50 nm, meanwhile, Al1000, Cr1000 and Mn1000 presented bigger hexagonal shaped-particles with an average grain size in the range of 1-2 µm. The observed $BaBiFe_{11}O_{19}$ morphology is associated to of Bi^{3+} substitution which promotes the formation of homogeneous spherical shapes, as it has been already reported [24].

The energy dispersive X-ray analysis (EDX) is carried out in order to confirm the chemical composition of the substituted hexaferrites. Fig. 4 shows the typical EDX spectra of substituted barium hexaferrite calcined at 1000 °C. The analysis data is collected in a table as inset in the same figure. The difference between the data in the two columns is discussed according to the atomic number of each element [25].

The estimated atomic percentages for different atoms basically agree with the designed composition. It is observed that the elements Ba, Fe, O and substituting trivalent ion are evenly distributed throughout the whole area, revealing a uniform chemical phase. The determined atomic ratio of Al, Cr, Bi and Mn to Fe is 0.120, 0.066, 0.09 and 0.106, respectively, which is close to the nominal value of 0.09 and within the uncertainty of the instrument.

3.4. Magnetic analysis

The room temperature magnetic hysteresis loops (M-H) of $BaFe_{12}O_{19}$ and $Ba\mathit{Me}Fe_{11}O_{19}$ (*Me*= Al, Bi, Cr and Mn) samples annealed at 900, 950 and 1000 °C for 2 h are shown in Fig. 6 and 7. The measured values of coercivity Hc, saturation magnetization Ms and remanent magnetization Mr are given in Table 4. According to ferromagnetic theory, magnetism in ferrites originates from the magnetic moments of ions in spin up and spin down orientations in sublattice [26]. Usually, the magnetic behaviour of the M-type hexaferrite is related to the distribution of iron ions in the crystallographic lattice sites. The Fe^{3+} ions are spread over five crystallographic sites: three octahedral sites 12k (spin up), 2a (spin up), and $4f_2$ (spin down), one tetrahedral $4f_1$ (spin down) and one bipyramidal 2b (spin up) as shown in Fig. 5 [27]. The magnetic moment of barium hexaferrite is deduced from the algebraic sum of iron magnetic moments in different positions according to [28]

$$M = M\,(12k + 2b + 2a) \uparrow\ - M\,(4\,f_1 + 4\,f_2\,) \downarrow$$

For undoped $BaFe_{12}O_{19}$, as the magnetic moment of Fe^{3+} is $5\mu_B$, the resulting magnetic moment is equal to 20 μ_B per unit formula leading to a magnetic moment of $40\mu_B$ per unit cell.

As observed in Fig. 7 and Table 4, the obtained samples have a ferromagnetic behaviour with magnetic properties affected by magnetic nature of trivalent ion substitutions and their occupied position in the five different lattice sites of Fe^{3+}. For non-magnetic substitution by Al^{3+} and Bi^{3+} ions, a significant reduction of Ms and Mr can be observed. Al^{3+} ions preferentially occupy the octahedral sites 12k (upward) [29, 30]. This preferential occupation results in a reduction of saturation magnetization. Bismuth atoms seek to replace $4f_1$ tetrahedral sites. As it is already discussed in XRD and FTIR section, Bi^{3+} is unstable in Fe^{3+} sites and can be oxidized to Bi^{5+} to enter the lattice [31, 32]. Consequently, two Fe^{2+} can be formed resulting in a decrease of Ms.

In case of magnetic substitution by Cr^{3+} and Mn^{3+} ions, the increase of Ms and Mr with calcination temperature is due to the decrease or disappearance of secondary phase as shown in X-ray diffraction patterns in Fig. 1. c. At calcination temperature higher than 900°C, no significant decrease in Ms and Mr values is observed compared to those of pure hexaferrite. As reported in the literature, Cr^{3+} with $3\mu_B$, at high substitution level (> 0.4), preferentially occupies 12k and 2a octahedral sites where it replaces Fe^{3+} [33, 34]. Consequently, the magnetic moment per formula unit M decreases which explains the observed slight decrease of magnetization. In manganese substituted BaM, Mn^{3+} ions may substitute the Fe^{3+} ions in all sites: 12k, 2a, 2b (spin up) or $4f_1$, $4f_2$ (spin down) [35, 36]. The replacement of Fe^{3+} by Mn^{3+} ions does not alter the saturation

magnetization because both have the same magnetic moment (as shown in Table 3, [37]).

Table 4 shows the variation of coercivity of doped barium hexaferrites upon annealing temperature and ion substitution. The substituted samples have larger coercivity than pure $BaFe_{12}O_{19}$ (0.241 T) which decreases with annealing temperature. The enhancement in coercivity is due partially to the smaller crystallite size [38]. As seen in XRD study, the *D* value of barium hexaferrite is reduced with the substitution (Table 1), but this fact alone cannot explain enhancement of Hc in Mn and Bi substituted samples. As Mn^{3+} and Fe^{2+} (induced by Bi^{5+}) are in the electronic configuration $3d^4$ and $3d^6$, respectively, they may bring significant orbital moment and contribute to the increase magnetorystalline anisotropy.

In order to determine the efficiency of a magnetic material, maximum energy product $(BH)_{max}$ is calculated using the magnetic data [39]. The evolution of $(BH)_{max}$ with substitution ions and calcination temperature is presented in Fig. 8. An increase of magnetic energy is well observed with increasing calcination temperature for all substituted barium ferrites except for $BaBiFe_{11}O_{19}$ which displays a remarkable decrease. It is also noted that the behaviour of $(BH)_{max}$ is related to the magnetic moment of trivalent ion. In fact, among magnetic ion substitutions, barium hexaferrite substituted with manganese ($5\mu_B$) reveals the highest energy product with 7.47 $kJ.m^{-3}$, meanwhile, for nonmagnetic ion substitutions, Aluminium substitution ($0\mu_B$) presents the lowest $(BH)_{max}$ with 4.40 $kJ.m^{-3}$, at 1000°C.

The maximum energy product reduction of bismuth substitution can be associated with the presence of the distortion created by two-steps hysteresis loop at all annealing

temperatures (Fig. 7. b) which is not due to the presence of secondary phase, as confirmed by XRD and FTIR data.

3.5. Curie point measurement

In order to figure out Curie temperature (T_c) of different substituted barium hexaferrites, temperature dependence of magnetization is measured using VSM with high temperature attachment. The magnetization of the samples is determined in the temperature range of 25 - 550 °C in an applied field of 1 T. Magnetization as function of temperature for different substitutions is shown in Fig. 9.

As it is clearly seen from the data, for all substituted ferrites, only one ferromagnetic - paramagnetic phase transition is observed which suggests the presence of single phase material as already indicated by diffraction patterns and infrared results. As presented in Table 5, T_c of $BaFe_{12}O_{19}$ is found to be 457 °C which is close to the value of 473 °C reported by Smit and Wijn [1]. It is interesting to note that Curie temperatures of Al, Cr and Bi doped hexaferrite sample are higher than that of pure $BaFe_{12}O_{19}$, whereas, $BaMnFe_{11}O_{19}$ revealed a lower Tc corresponding (Table 5). The change in Curie temperature is ascribed to the modification of the exchange strength of octahedral and tetrahedral interactions as consequence of a change of the trivalent ion distribution between these two sites [40].

From ions distribution, it is expected for Al^{3+}, Bi^{3+} and Cr^{3+} substitution with low magnetic moment replacing Fe^{3+} to decrease the strength of octahedral and tetrahedral interactions leading to decrease of Tc. However, Tc is found to increase. This can be attributed to the big ionic radius of aluminium, bismuth and chromium causing the distortion of lattice sites which is directly proportional to interionic distances. This

distortion leads to greater cation-anion-cation bond angles and strengthening of sites exchange interactions [41].

In the manganese substituted ferrite, the reduction of Curie temperature shown in Fig. 9 and Table 5, can be explained by the distribution of manganese ions over octahedral and tetrahedral sites. Producing, a shift of Curie temperature towards lower temperature, as observed in manganese substituted spinels and W-hexaferrites [1].

4. Conclusion

M-type hexaferrites Ba*Me*$Fe_{11}O_{19}$ substituted with trivalent nonmagnetic ions (Al^{3+}, Bi^{3+}) and magnetic ions (Cr^{3+}, Mn^{3+}) are successfully synthesized by dynamic hydrothermal technique. The XRD and FTIR analysis confirmed the formation of single phase hexagonal structure for all hexaferrites. Morphological investigation revealed small spherical-shaped particles (400 ± 50 nm) for Bi substitution and hexagonal-shaped particles (1-2 µm) for Al, Cr and Mn substitutions. The elemental study obtained from EDX analysis gave a uniform chemical composition for all samples. The magnetic study indicated that magnetic parameters markedly depend on the nature, concentration and distribution of doped ions on the five sites in the crystal lattice. The saturation magnetization decreased and the coercive field increased with nonmagnetic Al substitution as it preferred to occupy 12k sites. FTIR, DRX and magnetic characterization revealed that bismuth ions substituted iron ions at octahedral sites resulting to valence variation of Bi^{3+} to Bi^{5+} and Fe^{3+} to Fe^{2+} cations in the hexagonal structure which contributed to the modification of the magnetorystalline anisotropy, as seen from hysteresis loops. The magnetic properties (Ms, Mr and Hc and $(BH)_{max}$) of the hexaferrites decreased with nonmagnetic trivalent ions (Al^{3+}, Bi^{3+}) substitution and

increased with magnetic ions (Cr^{3+}, Mn^{3+}) substitution compared to pure $BaFe_{12}O_{19}$. Manganese ions, on other hand, replaced the Fe^{3+} ions in all five sites contributing to reach the maximum values of magnetization (Ms = 61.10 emu/g), remanence (Mr = 33.16 emu/g) coercivity (Hc = 0.430 T) inducing a greater maximum energy product ($(BH)_{max}$ = 7.47 $kJ.m^{-3}$). Accordingly, the substitution of Fe^{3+} by these trivalent ions at different sites is found to be affected by hydrothermal synthesis.

Acknowledgements

Authors are thankful to Université de Tunis El Manar, Tunis for the financial support to achieve this work and grateful for the funding obtained in the framework of scholarship for international students at SATIE, ENS de Cachan for 12 months.

References

[1] N.A. Spaldin, Magnetic materials fundamentals and applications, second edition, University press, The Edinburgh Building, Cambridge, (2010).

[2] C. Heck, Magnetic materials and their applications, 1st edition, Butterworths and co, England, (1974).

[3] R.C. Pullar, Hexagonal ferrites: a review of the synthesis, properties and applications of hexaferrite ceramics, Prog. Mater. Sci. 57 (2012) 1191-1334.

[4] L.A. Bashkirov, Yu. L Kostyushko, Formation of ferrite-chromites $BaFe_{10}Cr_2O_{19}$ and $SrFe_{10}Cr_2O_{19}$ in the solid-phase reaction of Fe_2O_3 and Cr_2O_3 with barium or strontium carbonate, Russ J. Appl. Chem. 78 (2005) 351-355.

[5] Y. Liu, M.G.B. Drew, J. Wang, M. Zhang, Y. Liu, Efficiency and purity control in the preparation of pure and/or aluminum-doped barium ferrites by hydrothermal methods using ferrous ions as reactants ,J. Magn. Magn. Mater. 322 (2010) 366-374.

[6] N.J. Shirtcliffe, S. Thompson, E.S. O'Keefe, S. Appleton, C.C. Perry, Highly aluminium doped barium and strontium ferrite nanoparticles prepared by citrate auto-combustion synthesis, Mater. Res. Bull. 42 (2007) 281-287.

[7] M.V. Rane, D. Bahadur, S.K. Mandal, M.J. Patni, Characterization of $BaFe_{12-2x}Co_xZr_xO_{19}$ ($0 \leq x \leq 0.5$) synthesised by citrate gel precursor route, J. Magn. Magn. Mater. 153 (1996) L1-L4.

[8] H. Yamamoto, M. Isono, T. Kobayashi, Magnetic properties of Ba–Nd–Co system M-type ferrite fine particles prepared by controlling the chemical coprecipitation method, J. Magn. Magn. Mater. 295 (2005) 51-56.

[9] C.A. Stergiou, I. Manolakis, T.V. Yioultsis, G. Litsardakis, Dielectric and magnetic properties of new rare-earth substituted Ba-hexaferrites in the 2–18 GHz frequency range, J. Magn. Magn. Mater. 322 (2010) 1532-1535.

[10] M. Ferrari, L. Lutterotti, Method for the simultaneous determination of anisotropic residual stresses and texture by X-ray diffraction, J. Appl. Phys. 76 (1994) 7246-7255.

[11] R. D. Shannon, Revised effective ionic radii and systematic studies of interatomic distances in halides and chalcogenides, Acta Cryst. (1976) 751-767.

[12] Y.Q. Jia, Crystal radii and effective ionic radii of the rare earth ions, J. Solid State Chem. 95 (1991) 184-187.

[13] J. Qiu, M. Gu, H. Shen, Microwave absorption properties of Al- and Cr-substituted M-type barium hexaferrite, J. Magn. Magn. Mater. 295 (2005) 263-268.

[14] Q. Fang, H. Ceng, K. Huang, J. Wang, R. Li, Y. Jiao, Doping effect on crystal structure and magnetic properties of chromium-substituted strontium hexaferrite nanoparticles, J. Magn. Magn. Mater. 294 (2005) 281-286.

[15] I.K. Lee, J.C. Sur, I.B. Shim, C.S. Kim, The effect of manganese substituted M-type hexagonal Ba-ferrite, J. Magnetics 14 (2009) 93-96.

[16] G. Asghar, M. Anis-ur-Rehman, Structural, dielectric and magnetic properties of Cr–Zn doped strontium hexa-ferrites for high frequency applications, J. Ally. Compd. 526 (2012) 85–90.

[17] M. Pal, P. Brahma, D. Chakravorty, D.C. Agrawal, Magnetic properties of Ba hexaferrites doped with bismuth oxide, J. Magn. Magn. Mater. 147 (1995) 208-212.

[18] F.M.M. Pereira, C.A.R Junior, M.R.P. Santos, R.S.T.M. Sohn, F.N.A. Freire, J.M. Sasaki, J.A.C. De Paiva, A.S.B. Sombra, Structural and dielectric spectroscopy studies of the M-type barium strontium hexaferrite alloys ($Ba_xSr_{1-x}Fe_{12}O_{19}$), J. Mater. Sci. Mater. Electron. 19 (2008) 627–638.

[19] Z. Mosleh, P. Kamelin , M. Ranjbar, H. Salamati, Effect of annealing temperature on structural and magnetic properties of $BaFe_{12}O_{19}$ hexaferrite nanoparticles, Ceram. Int. 40 (2014) 7279–7284.

[20] X. Tang, B.Y. Zhao, K.A. Hu, Preparation of M-Ba-ferrite fine powders by sugar-nitrates process, J. Mater. Sci. 41 (2004) 3867-3871.

[21] G.R. Gordani, A. Ghasemi, A. Saidi, Enhanced magnetic properties of substituted Sr-hexaferrite nanoparticles synthesized by co-precipitation method, Ceram. Int. 40 (2014) 4945–4952.

[22] S. Singhal, T. Namgyal, J. Singh, K. Chandra, S. Bansal, A comparative study on the magnetic properties of $MFe_{12}O_{19}$ and $MAlFe_{11}O_{19}$ (M = Sr, Ba and Pb) hexaferrites with different morphologies, Ceram. Int. 37 (2011) 1833-1837.

[23] S. Ram, Observation of enhanced dielectric permittivity in Bi^{3+} doped $BaFe_{12}O_{19}$, j. Magn. Magn. Mater. 80 (1989) 241-245.

[24] M.M. Eltabeya, W.R. Agamic, H.T. Mohsenb, Improvement of the magnetic properties for Mn–Ni–Zn ferrites by rare earth Nd^{3+} ion substitution, J. Adv. Res. 5 (2014) 601–605

[25] L. Qiao, B, Xu, Q. Xi, J. Zheng, L. Jiang, Effects of trace of Bi_2O_3 addition on the morphology of strontium ferrite particles, Ceram, Int. 36 (2010) 1423–1427.

[26] L. Néel, Magnetic properties of ferrites: ferrimagnetism and anti-ferromagnetism, Ann. Phys. Paris 3 (1948) 137-198.

[27] J. Smit, H.P.J. Wijn, Intrinsic properties of ferrites with hexagonal crystal structure, Chapter IX, in Ferrites, N.V Philips' Gloeilampenfabrieken, Eindhoven (Holland), (1959), 177-211.

[28]A. Ghasemi, A. Morisako, Static and high frequency magnetic properties of Mn–Co–Zr substituted Ba-ferrite, J. Alloy. Compd. 456 (2008) 485-491.

[29] M.N. Ashiq, M.J. Iqbal, I.H. Gul, Effect of Al–Cr doping on the structural, magnetic and dielectric properties of strontium hexaferrite nanomaterials, J. Magn. Magn. Mater. 323 (2011) 259-263.

[30] H.Z. Wanga, B. Yaoa, Y. Xua, Q. Hea, G.H. Wena, S.W. Longa, J. Fana, G.D. Lib, L. Shanb, B. Liua, L.N. Jianga, L.L. Gaoa, Improvement of the coercivity of strontium hexaferrite induced by substitution of Al^{3+} ions for Fe^{3+} ions, J. Ally. Compd. 537 (2012) 43-49

[31] T. Osotchan, S. Thongmee, I.M. Tang, On the coercivity of the Bi-doped Ba-hexaferrite $BaFe_{12-x}Bi_xO_{12}$, Thammasa Int. J. Sc .Tech. 4 (1999) 54-58.

[32] Y. Peng, X. Wu, Z. Chen, W. Liu, F. Wang, X. Wang, Z. Feng, Y. Chen, V.G. Harris, $BiFeO_3$ tailored low loss M-type hexaferrite composites having equivalent

permeability and permittivity for very high frequency applications, J. Ally. Compd. 630 (2015) 48-53

[33] Q. Fang, H. Cheng, K. Huang, J. Wang, R. Li, Y. Jiao, Doping effect on crystal structure and magnetic properties of chromium-substituted strontium hexaferrite nanoparticles, J. Magn. Magn. Mater. 294 (2005) 281-286.

[34] M. Awawdeh, I. Bsoul, S.H. Mahmood, Magnetic properties and Mössbauer spectroscopy on Ga, Al, and Cr substituted hexaferrites, J. Ally. Compd. 585 (2014) 465-473

[35] H. Fu, H.R. Zhai, Y.C. Zhang, B.X. Gu, J.Y. Li, Magnetic properties of Mn substituted barium ferrite, J. Magn. Magn. Mater. 54-57 (1986) 905-906.

[36] H. Sözeria, H. Deligözb, H. Kavasc, A. Baykald, Magnetic, dielectric and microwave properties of M-Ti substituted barium hexaferrites (M=Mn^{2+}, Co^{2+}, Cu^{2+}, Ni^{2+}, Zn^{2+}), Ceram. Int. 40 (2014) 8645-8657.

[37] E. C. Stoner, Magnetism and matter, Methucn and Co., London, (1934).

[38] E.C. Stoner, E.P. Wohlfarth, A mechanism of magnetic hysteresis in heterogeneous alloys, Philos. Trans. Roy. Soc. London Ser. A, Math. Phys. Eng. Sci. 240 (1948) 599-642.

[39] J.M.D. Coey, Magnetism and magnetic materials, first edition, Cambridge, University press, New York, (2009).

[40] H. Wijn, Landolt Bornstein III BD, 4b, Springer Verlag, Berlin, Heidelberg, New York, (1970), p.547.

[41] A. Guinier; W.J Duffin, R. Jullien, The solid state from superconductors to superalloys, Oxford: Oxford Univ. Press, (1989).

Tables

Table 1

Sample	Calcination Temperature (°C)	Abbreviation
$BaAlFe_{11}O_{19}$	900	Al900
	950	Al950
	1000	Al1000
$BaBiFe_{11}O_{19}$	900	Cr900
	950	Cr950
	1000	Cr1000
$BaCrFe_{11}O_{19}$	900	Cr900
	950	Cr950
	1000	Cr1000
$BaMnFe_{11}O_{19}$	900	Mn900
	950	Mn950
	1000	Mn1000

Table 2

Sample	a (nm)	c (nm)	c/a	$\rho_{x\text{-}ray}$ (g cm^{-3})	D (nm)
$BaFe_{12}O_{19}$	0.58944	2.3231	3.9439	5.286	294.5
Al900	0.58965	2.3223	3.9384	5.152	160.7
Al950	0.58921	2.3209	3.9390	5.150	177.9
Al1000	0.58917	2.3181	3.9345	5.150	183.5
Bi900	0.58992	2.3210	3.9344	6.028	153.5
Bi950	0.58931	2.3205	3.9376	6.063	213.2
Bi1000	0.58929	2.3185	3.9343	6.063	229.8
Cr900	0.58992	2.3179	3.9291	5.288	198.2
Cr950	0.58917	2.3195	3.9368	5.278	248.2
Cr1000	0.58824	2.3212	3.9460	5.278	262.1
Mn900	0.58893	2.3175	3.9351	5.295	204.9
Mn950	0.58909	2.3188	3.9362	5.295	207.1
Mn1000	0.58924	2.3193	3.9360	5.295	215.1

Table 3

Ion	Ionic radius (pm)	Ionic magnetic moment (μ_B)
Fe^{3+}	67	5
Fe^{2+}	83	4
Al^{3+}	57	0
Bi^{3+}	96	0
Bi^{5+}	74	0
Cr^{3+}	64	3
Mn^{3+}	70	5

Table 4

Composition	μ_0Hc (T)	Ms (emu/g)	Mr (emu/g)	Mr/Ms
$BaFe_{12}O_{19}$	0.241	61.84	33.95	0.567
Al900	0.335	51.89	28.86	0.535
Al950	0.329	52.86	30.05	0.538
Al1000	0.339	54.98	32.25	0.556
Bi900	0.488	46.27	24.54	0.531
Bi950	0.481	47.72	25.43	0.530
Bi1000	0.376	49.50	25.84	0.522
Cr900	0.449	36.47	19.41	0.532
Cr950	0.345	55.61	29.22	0.525
Cr1000	0.230	60.33	35.68	0.581
Mn900	0.434	50.16	27.96	0.546
Mn950	0.431	51.68	28.45	0.551
Mn1000	0.426	61.10	33.26	0.550

Table 5

Sample	T_c (°C)
$BaFe_{12}O_{19}$	457
$BaAlFe_{11}O_{19}$	485
$BaBiFe_{11}O_{19}$	478
$BaCrFe_{11}O_{19}$	479
$BaMnFe_{11}O_{19}$	424

Figures Captions

Fig. 1. X-ray diffraction patterns of samples a) $BaAlFe_{11}O_{19}$, b) $BaBiFe_{11}O_{19}$, c) $BaCrFe_{11}O_{19}$ and d) $BaMnFe_{11}O_{19}$ calcined at different temperatures

Fig. 2. FTIR absorption spectra of substituted barium hexaferrite calcined at 1000 °C

Fig. 3. SEM images of a) Al1000, b) Bi1000, c) Cr1000 and d) Mn1000

Fig. 4. EDX patterns for a) Al1000, b) Bi1000, c) Cr1000 and d) Mn1000

Fig. 5. Unit cell of the barium hexaferrite

Fig. 6. Hysteresis curve (M-H) of $BaFe_{12}O_{19}$

Fig. 7. Hysteresis curves (M-H) of a) $BaAlFe_{11}O_{19}$. b) $BaBiFe_{11}O_{19}$ c) $BaCrFe_{11}O_{19}$ and d) $BaMnFe_{11}O_{19}$ calcined at different temperatures

Fig. 8. Variation of $(BH)_{max}$ with the calcination temperature for different hexaferrite powders

Fig. 9. Magnetization of substituted hexaferrites as function of temperature used to determine the Curie temperature

Fig. 1.

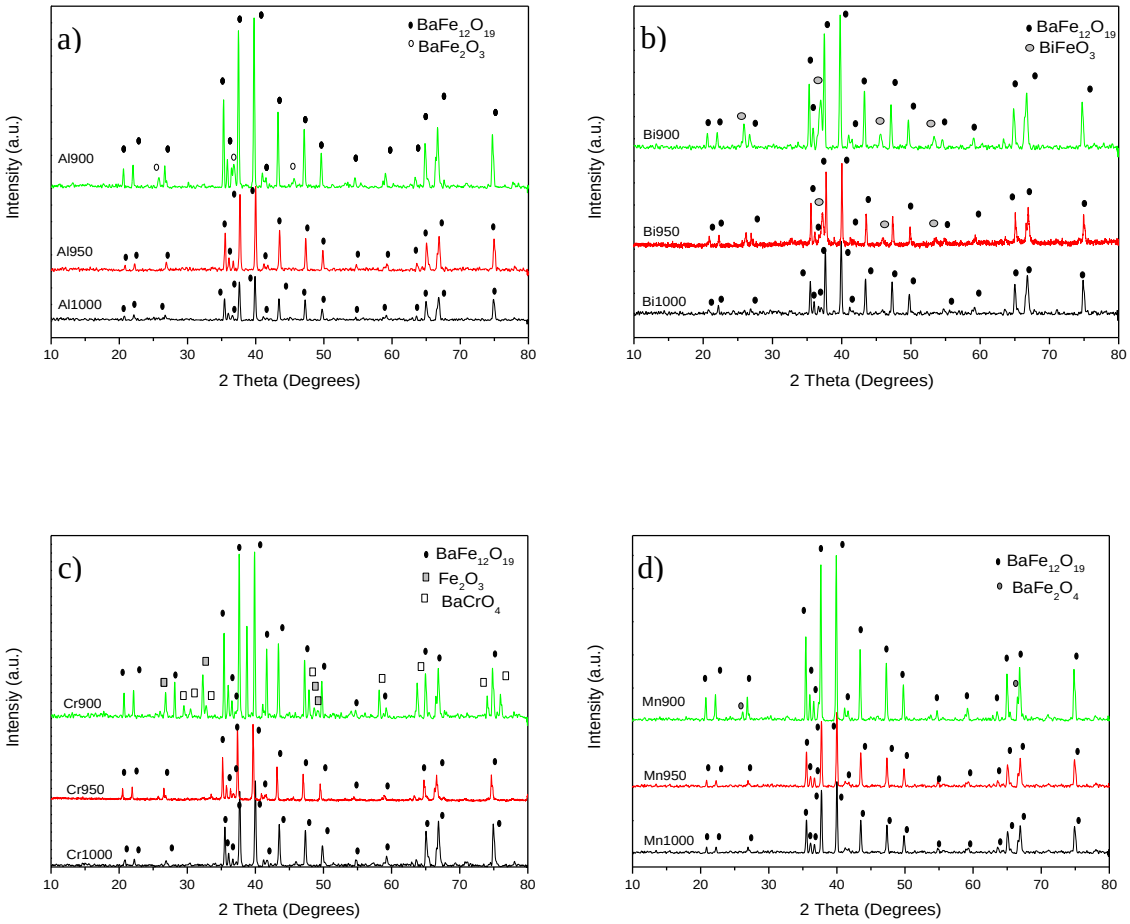
a)
BaFe12O19
BaFe2O3
Al900
Al950
Al1000
Intensity (a.u.)
2 Theta (Degrees)
b)
BaFe12O19
BiFeO3
Bi900
Bi950
Bi1000
Intensity (a.u.)
2 Theta (Degrees)
c)
BaFe12O19
Fe2O3
BaCrO4
Cr900
Cr950
Cr1000
Intensy (a.u.)
2 Theta (Degrees)
d)
BaFe12O19
BaFe2O4
Mn900
Mn950
Mn1000
Intensity (a.u.)
2 Theta (Degrees)

Fig. 2.

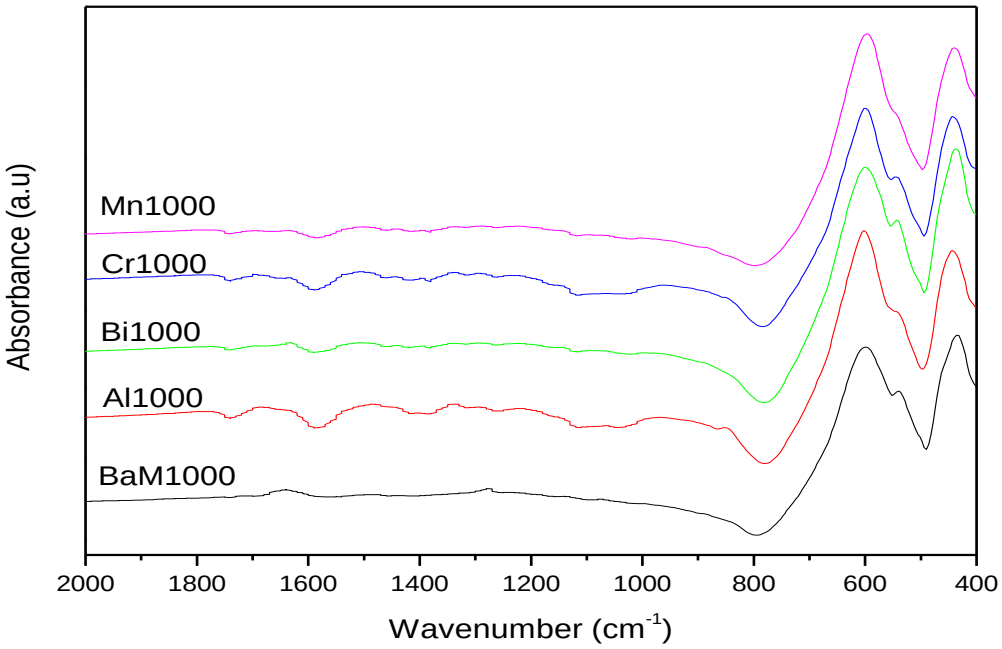
Absorbance (a.u)
Mn1000
Cr1000
Bi1000
Al1000
BaM1000
2000
1800
1600
1400
1200
1000
800
600
400
Wavenumber (cm-1)

Fig. 3.

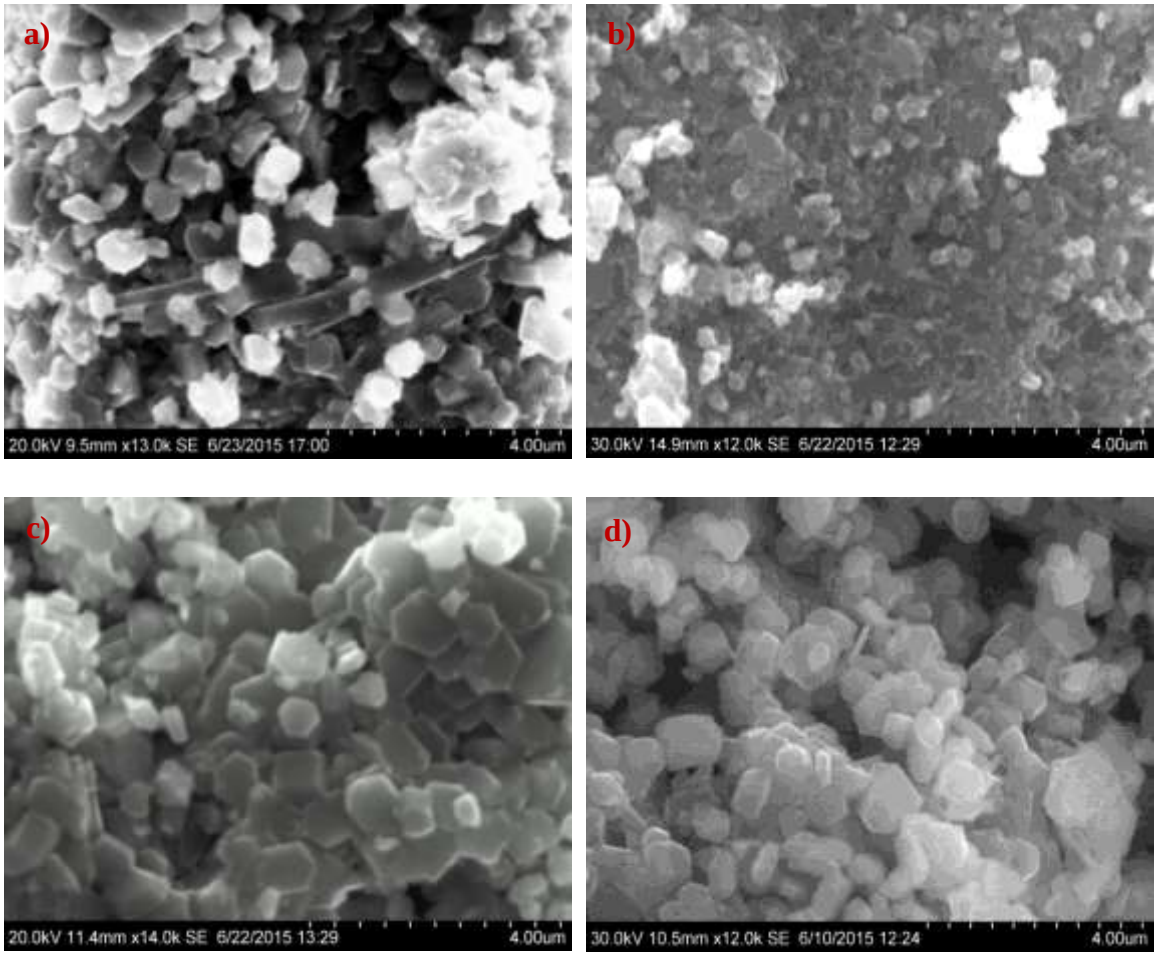
a)
20.0kV 9.5mm x13.0k SE 6/23/2015 17:00
4.00um
b)
30.0kV 14.9mm x12.0k SE 6/22/2015 12:29
4.00um
c)
20.0kV 11.4mm x14.0k SE 6/22/2015 13:29
4.00um
d)
30.0kV 10.5mm x12.0k SE 6/10/2015 12:24
4.00um

Fig. 4.

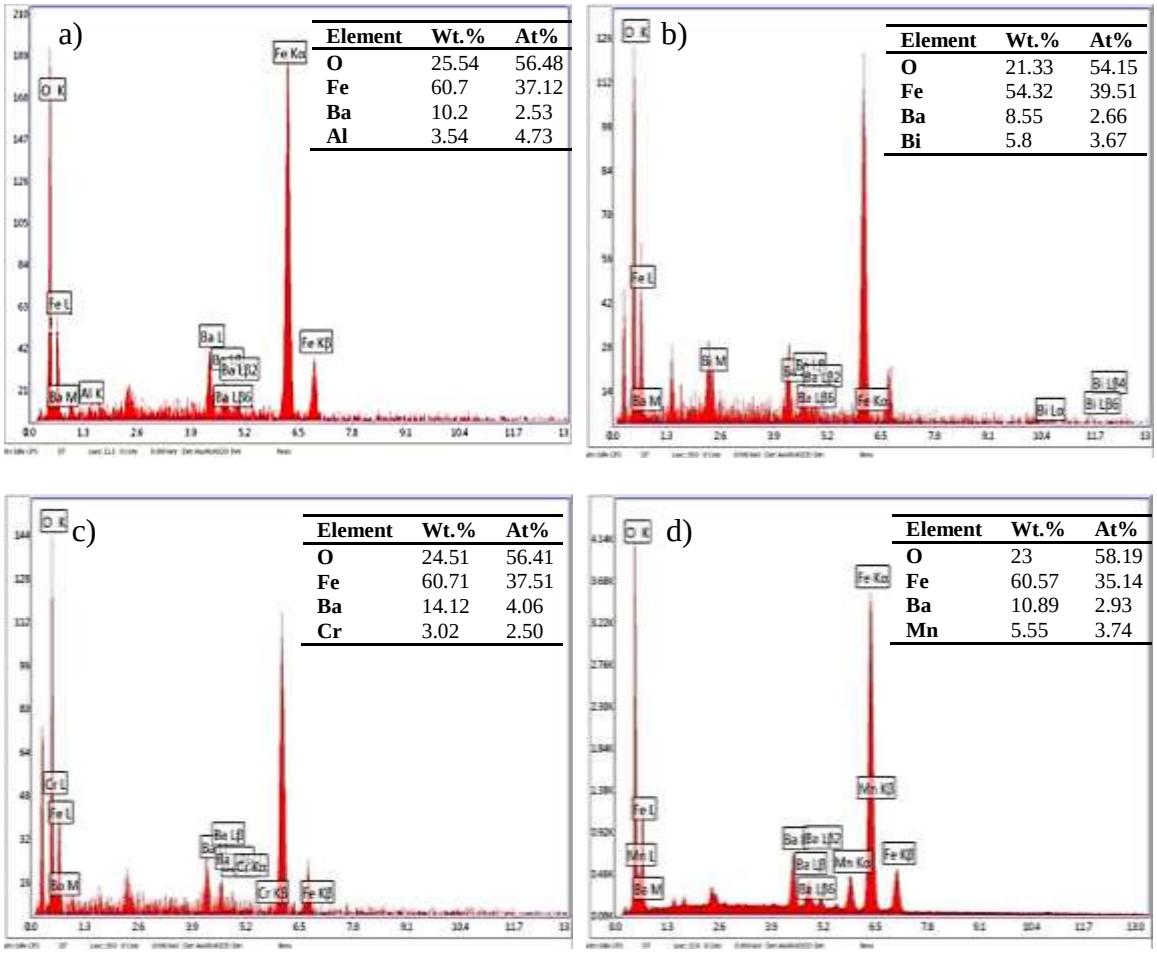

Element	Wt.%	At%
O	25.54	56.48
Fe	60.7	37.12
Ba	10.2	2.53
Al	3.54	4.73

Element	Wt.%	At%
O	21.33	54.15
Fe	54.32	39.51
Ba	8.55	2.66
Bi	5.8	3.67

Element	Wt.%	At%
O	24.51	56.41
Fe	60.71	37.51
Ba	14.12	4.06
Cr	3.02	2.50

Element	Wt.%	At%
O	23	58.19
Fe	60.57	35.14
Ba	10.89	2.93
Mn	5.55	3.74

Fig. 5.

Site	r (Å)	C	
⊞ Ba	1.42		
⊟ Fe	0.78		
Fe1	0.78		2a
Fe2	0.78		2b
Fe3	0.78		$4f_1$
Fe4	0.78		$4f_2$
Fe5	0.78		12k
⊞ O	1.00		

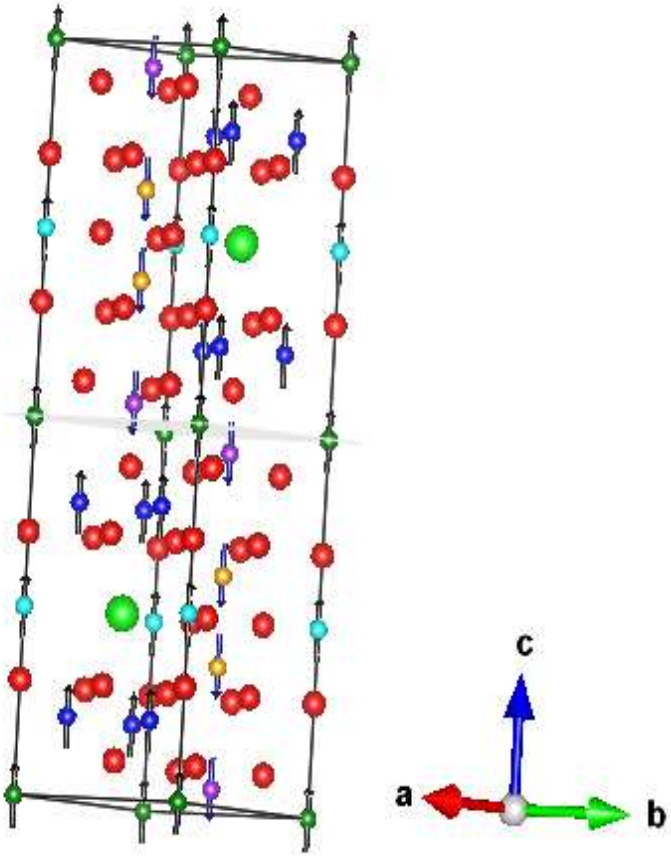

Fig. 6.

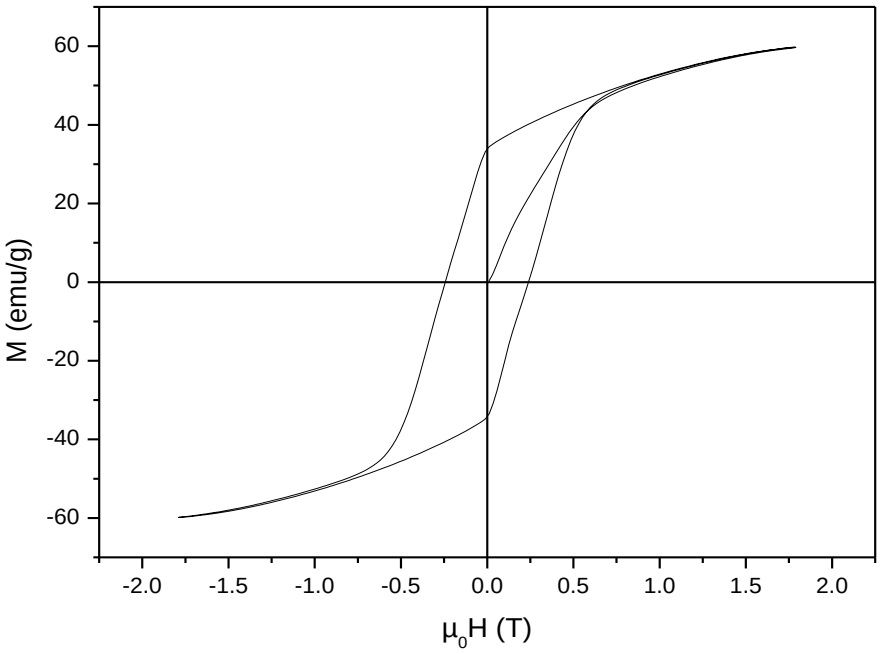

Fig. 7.

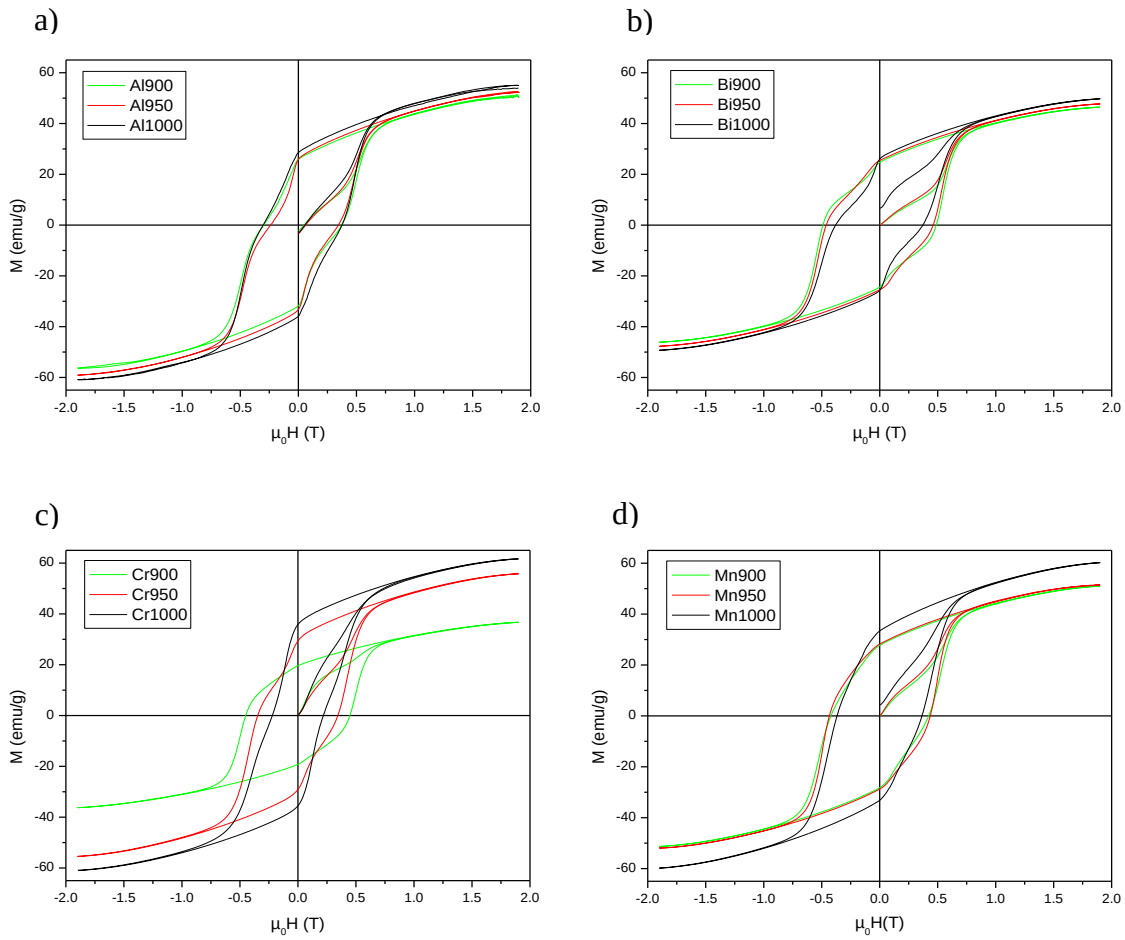
a)
Al900
Al950
Al1000
M (emu/g)
μ_0H (T)
b)
Bi900
Bi950
Bi1000
M (emu/g)
μ_0H (T)
c)
Cr900
Cr950
Cr1000
M (emu/g)
μ_0H (T)
d)
Mn900
Mn950
Mn1000
M (emu/g)
μ_0H(T)

Fig. 8.

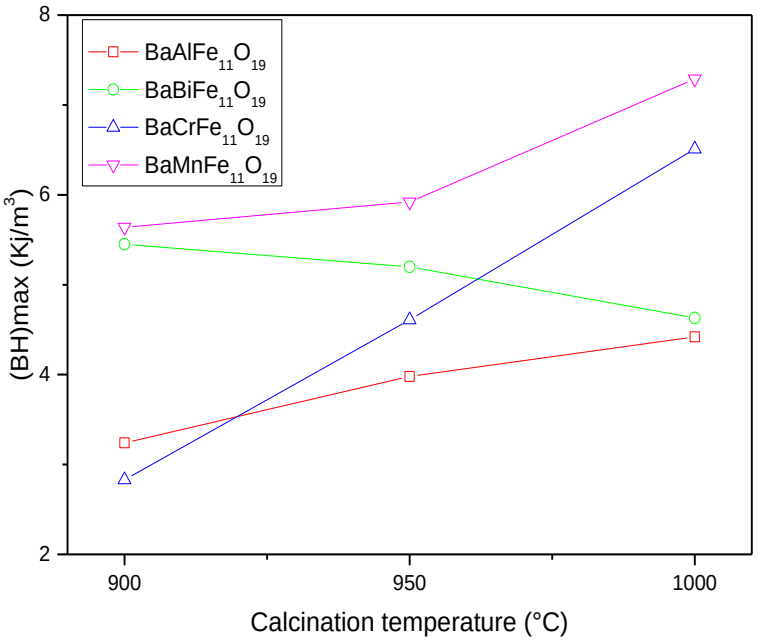
BaAlFe11O19
BaBiFe11O19
BaCrFe11O19
BaMnFe11O19
(BH)max (Kj/m3)
8
6
4
2
900
950
1000
Calcination temperature (°C)

Fig. 9

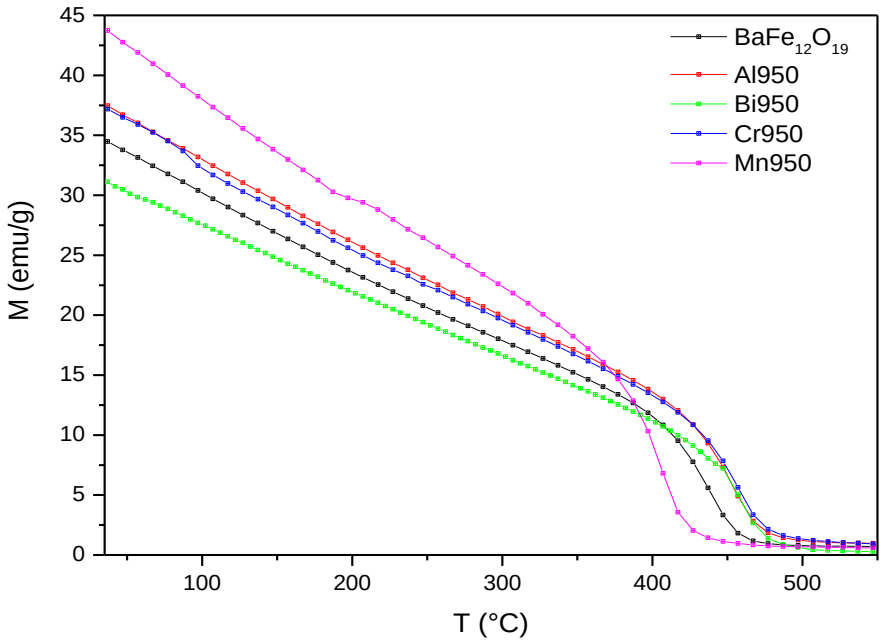
BaFe12O19
Al950
Bi950
Cr950
Mn950
M (emu/g)
T (°C)
0
5
10
15
20
25
30
35
40
45
100
200
300
400
500